Journal of Materials Chemistry C

Accepted Manuscript

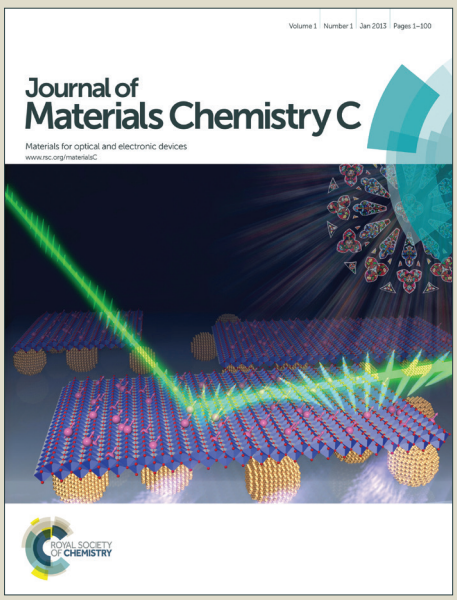

ROYAL SOCIETY OF CHEMISTRY

www.rsc.org/materialsC

From FePt-Fe_3O_4 to $L1_0$-FePt/Fe Nanocomposite Magnets with Gradient Interface

Weiwei Yang,[1] Wenjuan Lei,[1] Yongsheng Yu,[1, 2,3]* Wenlei Zhu, [2] T. A. George, [3] X.-Z. Li,[3] D. J. Sellmyer,[3] and Shouheng Sun[2]

[1] School of Chemical Engineering and Technology, Harbin Institute of Technology, Harbin, Heilongjiang 150001, China

[2] Department of Chemistry, Brown University, Providence, Rhode Island 02912, USA

[3] Nebraska Center for Materials and Nanoscience, University of Nebraska, Lincoln, Nebraska 68588, USA

E-mail: ysyu@hit.edu.cn

ABSTRACT

We report a novel approach for the fabrication of exchange-coupling $L1_0$-FePt/bcc-Fe nanocomposites with gradient interface between hard and soft phase from a facile one-pot synthesis of FePt nanoparticles (NPs) and FePt-Fe_3O_4 dumbbell NPs. High temperature annealing in Argon is first used to convert FePt in FePt-Fe_3O_4 dumbbell NPs to $L1_0$-FePt phase. Then Fe_3O_4 in FePt-Fe_3O_4 dumbbell NPs is reduced to bcc-Fe at low temperature annealing in reducing gas, forming $L1_0$-FePt/Fe nanocomposites. The $L1_0$-FePt/Fe nanocomposites exhibit both large coercivity and high magnetic moment. The work demonstrates that creating nanoscale gradient interface between magnetic hard and soft phases is a promising approach to the fabrication of high performance permanent magnets.

Keywords

$L1_0$-FePt/bcc-Fe, nanoparticles, exchange coupling, nanocomposite magnets

Introduction

To satisfy the fast growing demand for higher magnetic energy product, exchange-coupling nanocomposites have been introduced and demonstrated as a new generation of permanent magnets.[1, 2] Such composites are composed of magnetically hard and soft phases that are strongly coupled with the magnetization of the soft phase pinned along the hard phase direction and coercivity determined by the hard phase. They show a smooth, single phase-like hysteresis behavior and their maximum energy products, $(BH)_{max}$ can reach far beyond the limit of traditional single-phase magnets.[3-7] Conventional physical techniques have been explored to prepare exchange-coupling magnets.[8-13] However, the requirement that both the hard and soft phases are controlled at the nanometer scale, to ensure efficient exchange coupling, has posed significant preparation challenges. Self-assembly of nanoparticles (NPs) synthesized by chemical method has shown great advantages in controlling the size of the soft phase, a key parameter needed for efficient exchange-coupling between the hard and soft phases.[14-20]

FePt NPs are useful model building blocks for constructing permanent magnetic nanocomposites.[21-25] As a class of hard magnetic materials, FePt has a very large coercivity but a relatively low magnetic moment compared to other iron-based and magnetically soft Fe_3Pt or Fe. To obtain higher magnetic energy product, FePt and Fe_3O_4 NPs are co-assembled and the binary composite assemblies are annealed in a

reducing atmosphere to convert Fe_3O_4 to Fe and transform chemically disordered face-centered cubic (fcc) FePt, which is magnetically soft, to chemically ordered face-centered tetragonal (fct) FePt, which is magnetically hard.[26, 27] The annealing also removes the organic coating around each particle and allows interfacial diffusion between Fe and FePt, leading to nanocomposite $L1_0$-FePt/Fe_3Pt. In this process, two different kinds NP building blocks must be prepared separately and co-assembled. This is not only time consuming, but also difficult to control NP heterogeneity in the assembled structures to tune/maximize NP exchange coupling.

Because the magnetization of body-centered cubic (bcc) Fe is higher than that of Fe_3Pt, bcc-Fe is a better candidate as the soft phase to form exchange-coupling magnet. However, the $L1_0$-FePt tends to form a solid solution with Fe at high annealing temperature.[22, 26] As a result, $L1_0$-FePt/Fe is not in a thermodynamically stable state and cannot be produced easily. In this paper, we report a new approach for preparation of exchange-coupling $L1_0$-FePt/Fe nanocomposite magnets with gradient interface between hard phase and soft phase from a one-pot synthesis of monodisperse FePt and FePt-Fe_3O_4 dumbbell NPs with controllable morphology and compositions. Monodisperse FePt and FePt-Fe_3O_4 dumbbell NPs could be obtained by decomposition of $Fe(CO)_5$ and reduction of $Pt(acac)_2$ (acac = acetylacetonate) in a mixture of oleic acid (OA), oleylamine (OAm) and 1-octadecene (ODE). In the process, high temperature annealing in Argon is first used to convert FePt in FePt-Fe_3O_4 dumbbell NPs to $L1_0$-FePt phase. Then Fe_3O_4 in FePt-Fe_3O_4 dumbbell NPs is reduced to bcc-Fe at low temperature annealing in Ar + 5% H_2, forming

$L1_0$-FePt/Fe nanocomposites (**Scheme 1**). The $L1_0$-FePt/Fe nanocomposites exhibit both large coercivity and high magnetic moment. The work demonstrates that creating nanoscale gradient interface between magnetic hard and soft phases is a promising approach to the fabrication of high performance permanent magnets.

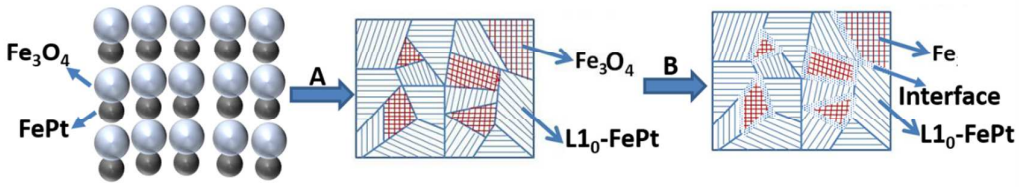

Scheme 1. Schematic illustration of the synthesis of $L1_0$-FePt/Fe nanocomposites by annealing FePt-Fe_3O_4 dumbbell NPs in (**A**) Argon at high temperature to convert FePt in FePt-Fe_3O_4 dumbbell NPs to $L1_0$-FePt phase and then (**B**) forming gas at low temperature to reduce Fe_3O_4 in FePt-Fe_3O_4 dumbbell NPs bcc-Fe.

Experimental

Chemicals and Materials

Oleylamine (OAm, >70%), 1-octadecene (ODE, technical grade, 90%), oleic acid (OA, technical grade, 90%), Pt(acac)2 (acac=aceylacetonate) (99%), iron pentacarbonyl ($Fe(CO)_5$, 99.9+% trace metals basis), hexane (98.5%), isopropanol (99.5%), ethanol (100%) were all purchased from Sigma Aldrich.

NPs Synthesis

$Pt(acac)_2$ (0.5 mmol), oleic acid (4 mmol), oleylamine (4 mmol), and 1-octadecene (10 mL)were mixed and magnetically stirred under a flow of nitrogen at room temperature. The solution was heated to 105 ^oC for 10 min to exclude moisture and ensure the dissolution of $Pt(acac)_2$. Under a blanket of nitrogen gas, 0.20 mL of $Fe(CO)_5$ was added at 120 ^oC. The solution was then heated to the synthesis

temperature at a heating rate of 5 ^{o}C/min, and kept at this temperature for 1 h. The heating source was then removed,and the solution was cooled to room temperature, after which the solution was exposed to air. A black product was precipitated by adding 40 mL of ethanol, and separated by entrifugation. The dark-yellow supernatant was discarded. The NPs were dispersed in 15 mL of hexane, and precipitated out by adding 20 mL of ethanol followed by centrifugation. The dispersion/ precipitation procedure was repeated three times. Finally, the production was re-dispersed in 10 mL of hexane.

Characterization

X-ray diffraction (XRD) characterization was carried out on a Bruker AXS D8-Advanced diffractometer with Cu K_{α} radiation (λ =1.5418 Å). The Inductively coupled plasma-atomic emission spectroscopy (ICP-AES) measurements were carried on a JY2000 Ultrace ICP Atomic Emission Spectrometer equipped with a JY AS 421 autosampler and 2400g/mm holographic grating. Samples for transmission electron microscopy (TEM) analysis were prepared by depositing a single drop of diluted clusters dispersion in hexane on amorphous carbon coated copper grids. TEM images were obtained with a Philips CM 20 operating at 200 kV. High-resolution TEM (HRTEM) images were obtained on a JEOL 2010 with an accerating votalage of 200 kV. The atomically resolved scanning transmission electron microscopy-EDS (STEM-EDS) images were obtained on a Fei Tecnai Osiris with an accerating votalage of 200 kV. Magnetic studies were carried out using a Quantum Design Superconducting Quantum Interface Device (SQUID) with a field up to 50 kOe at

room temperature.

Results and discussion

Figure 1 shows the representative TEM images of the NPs synthesized at different temperature. The pure FePt NPs were synthesized as reported[24] with a slight modification, in which 220 °C, instead of 240 °C, was used for the NPs growth. And **Figure 1A** is the typical TEM image of the 7 nm polyhedral $Fe_{49}Pt_{51}$ NPs synthesized at 220 ^{o}C. The NPs have a narrow size distribution with an average diameter of 7 ± 0.5 nm. When the synthesis temperature was increased to 260 ^{o}C, the dumbbell-like NPs could be found in the production, as shown in **Figure 1B**. With further increasing the synthesis temperature to 280 ^{o}C, more dumbbell-like NPs were formed (shown in **Figure 1C**). For the 300 ^{o}C synthesis, all the NPs has the dumbbell shape shown in **Figure 1D**. The HRTEM image of the dark part in the dumbbell shape NPs was shown in **Figure 1E** with the interfringe distance of 0.22 nm, corresponding to (111) plane spacing (0.220 nm) in fcc FePt structure. The HRTEM image of the light part in the dumbbell shape NPs was shown in **Figure 1F**.The interfringe distance was measured to be 0.31 nm, which is close to the lattice spacing of the (220) planes (0.30 nm) in the fcc Fe_3O_4 phase. These results suggest that the synthesis temperature is important in controlling the morphology of the NPs.

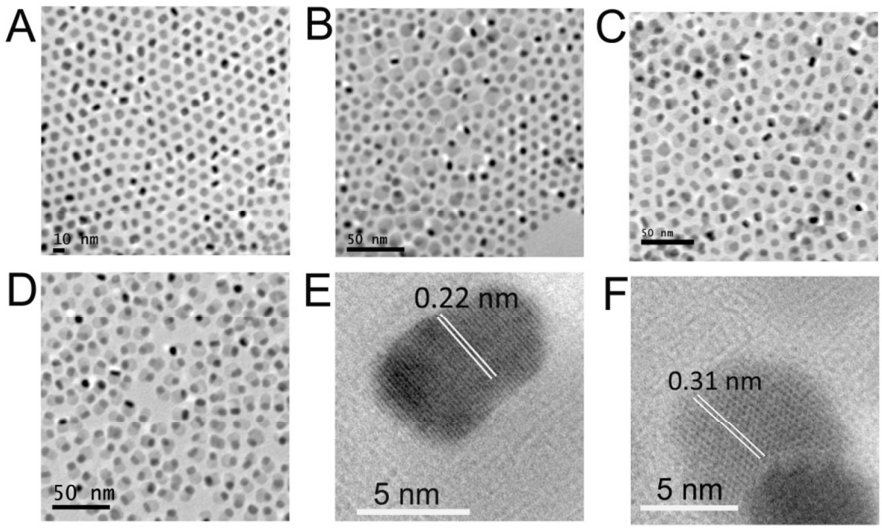

Figure 1. The representative TEM images of the NPs synthesized at different temperature: (**A**) 220 ^{o}C, (**B**) 260 ^{o}C, (**C**) 280 ^{o}C, (**D**) 300 ^{o}C, (**E**) HRTEM images of FePt in FePt-Fe_3O_4 dumbbell NPs, and (**F**) HRTEM images of Fe_3O_4 in FePt-Fe_3O_4 dumbbell NPs.

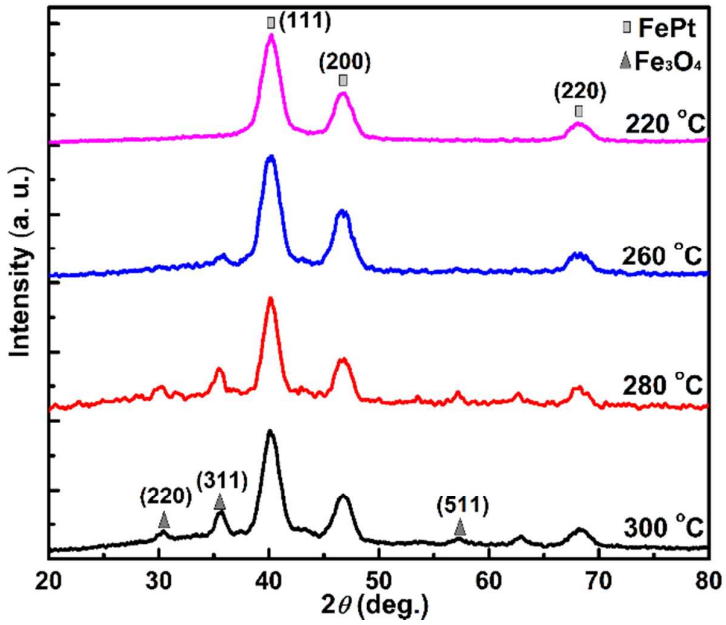

Figure 2. XRD patterns of the as-synthesized NPs synthesized at different temperature.

The formation of dumbbell in the synthesis can be characterized by XRD.

Figure 2 shows the XRD patterns of the as-synthesized NPs synthesized at different temperature. For the NPs synthesized at 220 ^{o}C, only (111) (200) and (220) peaks of fcc-FePt are observed. The average particle size estimated from (111) peak by Scherrer's formula is almost the same as that measured from the TEM image, indicating the single crystal nature in each individual FePt NP. Increasing the synthesis temperature to 260 ^{o}C, (311) peak of Fe_3O_4 phase appeared. When the NPs was synthesized at 280 and 300 ^{o}C, Fe_3O_4 peak intensity increases, suggesting more Fe_3O_4 formed in the dumbbell structure , which is consistent with the TEM observation.

By keeping the amount of $Pt(acac)_2$ and $Fe(CO)_5$ constant at 0.5 mmol and 0.2 mL (1.50 mmol) respectively and the $Fe(CO)_5/Pt(acac)_2$ precursor molar ratio (which was set to 3), we could control a Fe content in the as-synthesized NPs of 28 to 74% by simply changing the synthesis temperature and maintaining the reaction time for 1 h. **Figure S1** shows the correlation between the synthesis temperature and the final Fe content in the as-synthesized NPs. When the NPs were synthesized at 180 ^{o}C, the Fe content is 28%. And the Fe content increases with increasing the synthesis temperature. In the reaction, $Fe(CO)_5$ is thermally unstable and subject to decomposition at high temperature to carbon monoxide and Fe. And carbon monoxide can serve as a reducing agent to reduce $Pt(acac)_2$ to Pt. At the low synthesis temperature, Pt rich nuclei are formed from the reduction of $Pt(acac)_2$ and the slow decomposition of $Fe(CO)_5$. More Fe atoms then diffuse into existing Pt-rich nuclei with increasing the synthesis temperature, leading to the increase of the Fe content in

the as-synthesized NPs.[22] In the current reaction condition, the amount of $Fe(CO)_5$ is three times as that of $Pt(acac)_2$. From **Figure S1**, we can see that $Fe(CO)_5$ cannot be completely consumed at temperatures less than 300 °C. The rest of $Fe(CO)_5$ reacts with OAc to form Fe-oleate complex, which decomposes at high temperature and form Fe_3O_4 [28] that nucleate and growth on FePt NPs, forming dumbbell NPs, as shown in **Figure 1B**, **C** and **D**. When the synthesis temperature was increased to 300 ^oC, Fe content in the as-synthesized NPs increases to 74%, which is almost three times as that of Pt, indicating that all Fe-oleate complex decomposed at 300 ^oC. We also found that the decomposition of Fe-oleate complex is time dependent. **Figure S2** shows the relationship between the reaction time and the final Fe content in the NPs synthesized at 300 ^oC. When the reaction temperature was just increased to 300 ^oC, the Fe content is about 51%. In the first 20 min reaction, the Fe content increased quickly after which the Fe content increases slowly due to the near complete consumption of the Fe-oleate complex. Combined Figure **S1** and **S2**, we could found that Fe-oleate complex could partially decompose below 300 ^oC and will decompose quickly at 300 ^oC. The morphology evolution of NPs synthesized at 300 ^oC for different reaction time was monitored by TEM, as shown in **Figrue S3**. From **Figure S3A**, we can see that when the reaction solution reaches just 300 ^oC, the product separated from the reaction solution contains mostly the FePt NPs. More FePt-Fe_3O_4 dumbbell NPs are formed when the reaction proceeds for 5 min, as shown in **Figure S3B**. 10 min later, dumbbell NPs are the major product (**Figure S3C** and **D)**. These results are in accordance with the ICP results shown in **Figure S2**, which show

that more Fe_3O_4 nucleates on the surface of FePt NPs in the first 20 min reaction, leading to the quick increase of Fe content in the NP product.

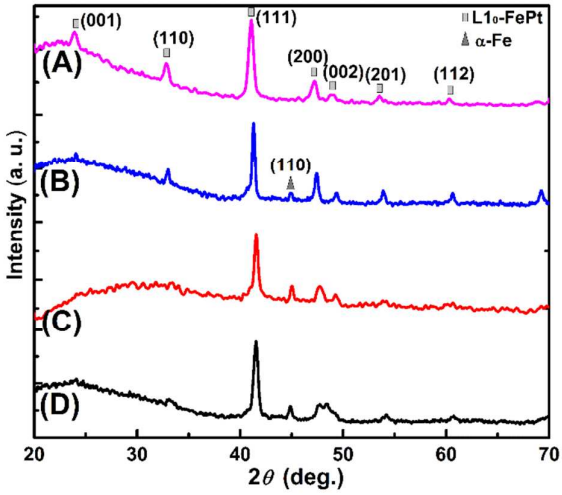

Figure 3. XRD patterns of the samples synthesized at different temperature: (A) 220 ^oC, (B) 260 ^oC, (C) 280 ^oC and (D) 300 ^oC after annealing at 600 ^oC for 1 h under Ar and at 350 ^oC for 4 h under Ar +H_2 (5%).

In order to obtain $L1_0$-FePt and bcc-Fe nanocomposites, the FePt and FePt-Fe_3O_4 NPs synthesized at different temperatures were first annealed at 600 ^oC for 1 h under Ar to convert fcc-FePt to fct-FePt, then at 350 ^oC for 4 h under Ar +H_2 (5%) to reduce Fe_3O_4 in FePt-Fe_3O_4 dumbbell NPs to bcc-Fe. **Figure 3** shows the typical XRD patterns of the samples annealed at 600 ^oC for 1 h under Ar and 350 ^oC for 4 h under Ar +H_2 (5%). After these two step annealing, the 220 ^oC synthesis sample shows (001), (110), (201) and (112) superstructure diffraction peaks and the fcc (200) diffraction peak is divided into fct (200) and fct (002) diffraction peaks. These results mean that the $L1_0$ phase is formed. For the annealed 260 ^oC synthesis sample, both $L1_0$-FePt phase and bcc-Fe ((110) peak) are seen in the XRD pattern. The relative intensities of the (110) peak of bcc-Fe increase with the fraction of dumbbell

FePt-Fe_3O_4 NPs present in the samples. These XRD patterns indicate that the two step annealing results in the conversion of the fcc FePt NPs to the $L1_0$-FePt, and Fe_3O_4 in FePt-Fe_3O_4 dumbbell NPs to α-Fe phase. It looks that the low temperature annealing in the second step is essential to preserve the Fe phase from its diffusion into $L1_0$-FePt. Therefore, $L1_0$-FePt/Fe nanocompostes are formed.

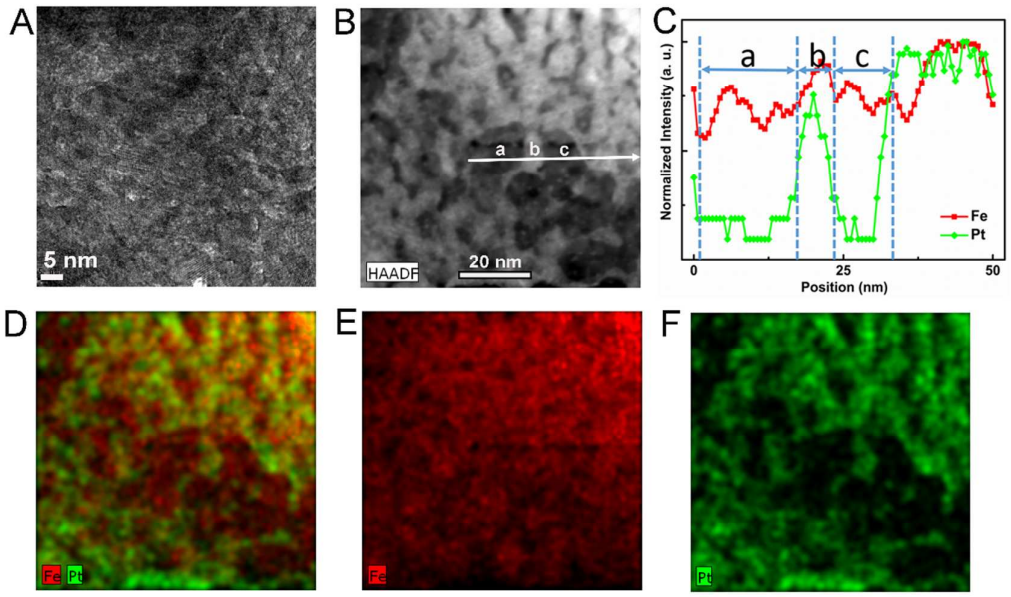

Figure4 (**A**) the typical TEM and (**B**) the HAADF images of $L1_0$-FePt and bcc-Fe nanocomposites. (**C**) the linear scan STEM-EELS result from (**B**). (**D-F**) Elemental mappings of Fe (red)/Pt (green) signals combined (**D**) and single element Fe (red) (**E**) and Pt (green) (**F**).

The nanocrystalline feature of both $L1_0$-FePt and bcc-Fe in the composites is characterized with TEM. **Figure 4A** shows the typical TEM image of the annealed $L1_0$-FePt/bcc-Fe composites (initial NPs synthesized at 260 ^oC). It can be seen that the nanoscale domains adopt different structural orientations, which means that nanograins are formed by two step annealing. Contrast variations in the high-angle

annular dark field (HAADF) images are proportional to the square of the element's atomic number and can therefore provide key information regarding the elemental distribution within nanostructures at subangstrom resolution. **Figure 4B** is the typical HAADF image of the nanocomposites, which shows the obvious light and dark contrast, indicating that the annealed samples contain two phases. The compositional architecture of the annealed samples was further measured by linear scan scanning transmission electron microscopy-EDS (STEM-EDS) from **Figure 4B**, as shown in **Figure 4C**. It can be clearly seen that dark areas a and c in **Figure 4B** are bcc-Fe phase and light area b is $L1_0$-FePt phase. The distributions of Pt at the interface from $L1_0$-FePt to bcc-Fe phase gradually decrease, which means that the interfaces between hard phase and soft phase are gradient. In other words, the continuously variation of Pt composition between the hard phase and soft phase produces the gradient interface, which usually leads to the continuously variation of the anisotropy between hard phase and soft phase.[29-31] **Figure 4D-F** show the elemental mapping results of Fe (red) and Pt (green) from **Figure 4B**, which also confirm that the light areas in **Figure 4B** are $L1_0$-FePt phase and the dark areas are bcc-Fe phase. These analyses suggest that $L1_0$-FePt/bcc-Fe nanocomposites with gradient interface between hard and soft phase are indeed formed from the two step annealing.

Magnetic measurements of the samples after two step annealing (600 ^{o}C for 1 h under Ar and then at 350 ^{o}C for 4 h under Ar +H_2 (5%)) were carried out using with a superconducting quantum interference device (SQUID) up to a maximum applied field of 50 kOe at room temperature. Magnetic hysteresis loops of the annealed

samples are shown in **Figure 5A**. After annealing, the hysteresis loop of the pure FePt NPs synthesized at 220 ^{o}C shows the hard magnetic properties with the coercivity of 14.52 kOe and saturated moment (M_s) about 44.1 emu/g. For the annealed sample synthesized at 260 ^{o}C and initially composed of FePt and FePt-Fe_3O_4 dumbbell NPs, the hysteresis loop still shows the single phase behavior and hard magnetic properties with 6.56 kOe coercivity and 72.7 emu/g saturated moment. From **Figure 5A**, we can see that M_s of the sample synthesized at 260 ^{o}C is much higher than that of the pure FePt NPs synthesized at 220 ^{o}C after annealing. These results also confirmed that bcc-Fe in the annealed sample could effectively enhance the saturated moment of the samples. Due to the single phase behavior of the hysteresis loop of the annealed sample, the dimension of the soft magnetic bcc-Fe phase should be smaller than twice the domain wall width of the hard magnetic phase and effective exchange coupling occurs within a two-phase magnet, which means that the annealed sample synthesized at 260 ^{o}C is exchange-coupling nanocomposite magnet with enhanced saturated moment. For the annealed sample from the pure FePt-Fe_3O_4 dumbbell NPs synthesized at 300 ^{o}C, although the hysteresis loop of the sample shows an enhanced saturated moment, an obvious two phase behavior is seen in the hysteresis loop, which means that the soft magnetic bcc-Fe phase should be larger than twice the domain wall width of $L1_0$-FePt phase and $L1_0$-FePt/bcc-Fe do not switch cooperatively. **Figure 5B** summarizes the synthesis temperature dependent M_s and H_c of the annealed samples. The H_c (M_s) of the NP assembly decreases (increases) with the synthesis temperatures, because the amount of bcc-Fe in the annealed samples

increases with increasing the synthesis temperature.

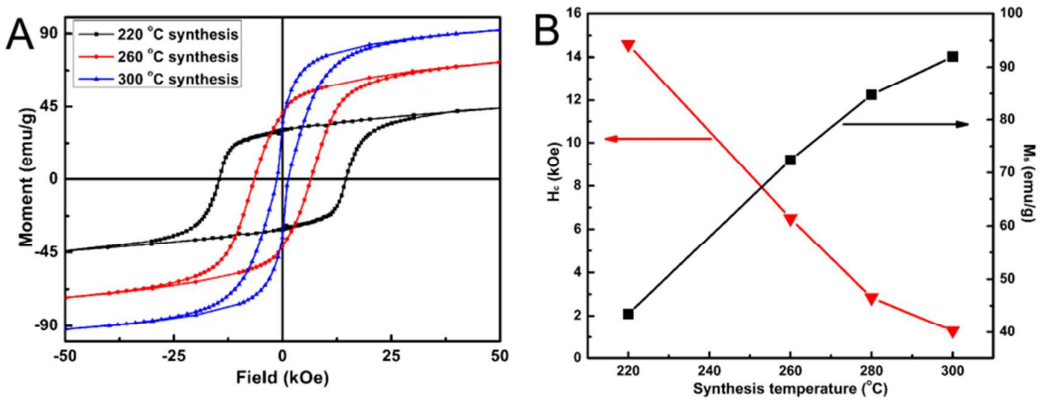

Figure 5. (**A**) the hysteresis loops of the samples synthesized at 220, 260 and 300 ^{o}C after 600 ^{o}C for 1 h under Ar and 350 ^{o}C for 4 h under Ar +H_2 (5%). (**B**) the synthesis temperature dependent M_s and H_c of the annealed samples.

In order to further characterize the exchange-coupling strength in the nanostructured permanent magnets, the recoil loops of the nanocomposites were measured.[29-35] The wide open recoil loops are usually observed in hard/soft exchange-coupling nanocomposite magnets while the recoil loops are usually narrow or even closed in single-phase magnets. **Figure 6** is the recoil loops of pure FePt NPs synthesized 220 ^{o}C and the mixture of FePt and FePt-Fe_3O_4 dumbbell NPs synthesized 260 ^{o}C after annealing. From **Figure 6A**, it was found that the recoil loops of pure FePt NPs synthesized 220 ^{o}C are almost closed and no hysteresis behavior was found in the recoil loops after, which means that the annealed sample only contains $L1_0$ FePt phase. In contrast to **Figure 6A**, we can see that recoil loops measured from the annealed sample initially composed of pure FePt and FePt-Fe_3O_4 dumbbell NPs are open and encompass a finite area, as shown in **Figure 6B**, which

are very similar to the recoil loops of exchange-coupling nanocomposites reported previously.[32-38] These results also confirmed that a two-phase structure, $L1_0$-FePt and bcc-Fe phase, is in annealed sample initially composed of pure FePt and FePt-Fe_3O_4 dumbbell structure.

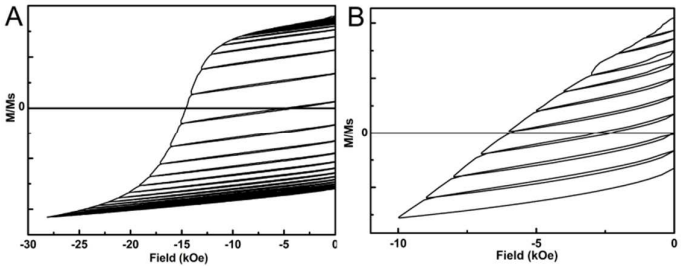

Figure 6. The recoil loops of (**A**) pure FePt NPs synthesized 220 ^oC and (**B**) the mixture of FePt and FePt-Fe_3O_4 dumbbell NPs synthesized 260 ^oC after annealing 600 ^oC for 1 h under Ar and 350 ^oC for 4 h under Ar +H_2 (5%).

Conclusion

In summary, a novel approach has been described for the fabrication of exchange-coupling $L1_0$-FePt/bcc-Fe nanocomposites with gradient interface between hard and soft phase from a facile one-pot synthesis of FePt NPs and FePt-Fe_3O_4 dumbbell NPs. These NPs are readily tuned from FePt NPs, even mixture of FePt NPs and FePt-Fe_3O_4 dumbbell NPs, to pure FePt-Fe_3O_4 dumbbell NPs by simply changing the synthesis temperature. After the high temperature annealing in argon, fcc FePt NPs in the as-synthesized samples could be converted into $L1_0$-FePt phase. And after the low temperature annealing in forming gas, Fe_3O_4 in FePt-Fe_3O_4 dumbbell NPs was reduced into bcc-Fe phase. After these two step annealing, exchange-coupling $L1_0$-FePt/bcc-Fe nanocomposites with gradient interface between hard and soft phase could be obtained. The reported one-pot synthesis plus two step annealing should

offer a general approach to exchanged-coupled $L1_0$-FePt/bcc-Fe nanocomposite magnets with high magnetic performance.

Acknowledgements

This work was supported by the National Natural Science Foundation of China under Grant (Nos. 51101069 and 21305025). The research at Brown University was supported by the U.S. Department of Energy, Office of Energy Efficiency and Renewable Energy (EERE), under its Vehicle Technologies Program, through the Ames Laboratory. The Ames Laboratory is operated by Iowa State University under contract DE-AC02-07CH11358. The research at Nebraska was supported by the US Department of Energy (Grant No. DE-FG02-04ER46152, magnetic characterization), the US Army Research Office (W911NF-10-2-0099, structural characterization), and NSF (NSF-DMR-0960110, major research instrumentation). The research was performed in part in central facilities of the Nebraska Center for Materials and Nanoscience (which is supported by the Nebraska Research Facilities).

References

1 R. Skomski, J. M. D. Coey *Phys. Rev. B,* 1993, **48**, 15812.

2 E. F. Kneller, R. Hawig, *IEEE Trans. Magn.,* 1991, **27**, 3588.

3 Y. Q. Wu, D. H. Ping, K. Hono, M. Hamano, A. Inoue *J. Appl. Phys.,* 2000, **87**, 8658.

4 J. P. Liu, C. P. Luo, Y. Liu, D. J. Sellmyer *Appl. Phys. Lett.,* 1998, **72**, 483.

5 X. Rui,; J. E. Shield, Z. Sun, Y. Xu, D. J. Sellmyer *Appl. Phys., Lett.,* 2006, **89**, 122509.

6 Y. L. Hou, S. H. Sun, C. B. Rong, J. P. Liu *Appl. Phys. Lett.,* 2007, **91**, 153117.

7 M. J. Kramer, R. W. McCallum, I. A. Anderson, S. Constantinides *J. Min. Met. Mat. Soc.,* 2012, **64**, 752.

8 X. Q. Liu, S. H. He, J. M. Qiu, and J. P. Wang *Appl. Phys. Lett.,* 2011, **98**, 222507.

9 B. Balamurugan, B. Das, V. R. Shah, R. Skomski, X. Z. Li, and D. J. Sellmyer *Appl. Phys. Lett.,* 2012, **101**, 122407.

10 W. B. Cui, Y. K. Takahashi, and K. Hono *Adv. Mater.,* 2012, **24**, 6530.

11 X. Rui, J. E. Shield, Z. Sun, R. Skomski, Y. Xu, D. J. Sellmyer, M. J. Kramer, Y.Q. Wu *J. Mag, Mag. Mater.,* 2008, **320**, 2576.

12 Y. Liu, T. A. George, R. Skomski, and D. J. Sellmyer *J. Appl. Phys.,* 2012, **111**, 07B537.

13 Y. Liu, T. A. George, R. Skomski, and D. J. Sellmyer *Appl. Phys. Lett.,* 2011, **99**, 172504.

14 T. Teranishi, Y. Inoue, M. Nakaya, Y. Oumi, T. Sano *J. Am. Chem. Soc.,* 2004, **126**, 9915.

15 Y. L. Hou, H. Kondoh, T. Kogure, T. Ohta *Chem. Mater.,* 2004, **16**, 5149.

16 T. Teranishi, M. Saruyama, M. Nakaya, M. Kanehara, *Angew. Chem., Int. Ed.,* 2007, **46**, 1713.

17 Y. L. Hou, Z. C. Xu, S. Peng, C. B. Rong, J. P. Liu, S. H. Sun *Adv. Mater.,* 2007, **19**, 3349.

18 A. Figuerola, A. Fiore, R. D. Corato, A. Falqui, C. Giannini, E. Micotti, A. Lascialfari, M. Corti, R. Cingolani, T. Pellegrino et al. *J. Am. Chem. Soc.,* 2008, **130**, 1477.

19 T. Teranishi, A. Wachi, M. Kanehara, T. Shoji, N. Sakuma, M. Nakaya *J. Am. Chem. Soc.,* 2008, **130**, 4210.

20 N. Sakuma, T. Ohshima, T. Shoji, Y. Suzuki, R. Sato, A. Wachi, A. Kato, Y. Kawai, A. Manabe, T. Teranishi, *Acs Nano,* 2011, **5**, 2806.

21 S. H. Sun, C. B. Murray, D. Weller, L. Folks, A. Moser *Science,* 2000, **287**, 1989.

22 S. H. Sun *Adv. Mater*., 2006, **18**, 393.

23 H. Zeng, J. Li, Z. L. Wang, J. P. Liu, S. H. Sun *Nano Lett.,* 2004, **4**, 187.

24 J. Kim, C. B. Rong, J. P. Liu, and S. H. Sun *Adv. Mater.,* 2009, **21**, 906.

25 J. M. Qiu, J. P. Wang *Adv. Mater.,* 2006, **19**. 1703.

26 H. Zeng, J. Li, J. P. Liu, Z. L. Wang, S. H. Sun *Nature*, 2002, **420**, 395.

27 J. Li, Z. L.Wang, H. Zeng, S. Sun, J. P. Liu *Appl. Phys. Lett*., 2003, **82**, 3743.

28 E. Kang, J. Park, Y. Hwang, M. Kang, J.-G. Park, and T. Hyeon *J. Phys. Chem. B,* 2004, **108**, 13932.

29 J. Lee, V. Alexandrakis, M. Fuger, B. Dymerska, D. Suess, D. Niarchos, and J. Fidler *Appl. Phys. Lett*. 2011, **98**, 222501.

30 Z. Lu, J. Guo, Z. Gan, Y. Liu, R. Xiong, G. J. Mankey, and W. H. Butler *J. Appl. Phys.* 2013, **113**, 073912.

31 J. Zhang, Z. Sun, J. Sun, S. Kang, S. Yu, G. Han, S. Yan, L. Mei, and D. L *Appl. Phys. Lett.* 2013, **102**, 152407.

32 A. Bollero, O. Gutfleisch, K.-H. Muller, L. Schultz, and G. Drazic *J. Appl. Phys.,* 2002, **91**, 8159.

33 C. L. Harland, L. H. Lewis, Z. Chen, and B. M. Ma *J. Magn. Magn. Mater.,* 2004, **271**, 53.

34 K. Kang, L. H. Lewis, J. S. Jiang, and S. D. *J. Appl. Phys.,* 2005, **98**, 113906.

35 C. B. Rong, V. Nandwana, N. Poudyal, Y. Li, J. P. Liu, Y. Ding, and Z. L. Wang *J. Phys. D,* 2007, **40**, 712.

36 Y. Choi, J. S. Jiang, J. E. Pearson, S. D. Bader, and J. P. Liu *Appl. Phys. Lett.,* 2007, **91**, 022502.

37 C. B. Rong, Y. Z. Liu, and J. P. Liu *Appl. Phys. Lett.,* 2008, **93**, 042508.

38 C. B. Rong and J. Ping Liu *J. Appl. Phys.,* 2009, **105**, 07A714.

Colour graphic:

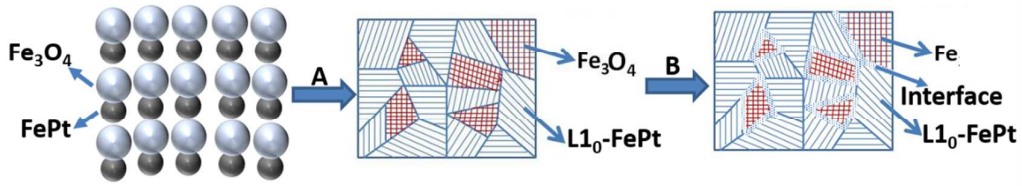

Text:

Exchange-coupling $L1_0$-FePt/bcc-Fe nanocomposites with gradient interface is obtained from annealing FePt and FePt-Fe_3O_4 dumbbell NPs